Enhancement of functional activity and biosynthesis of exopolysaccharides in *Monascus purpureus* by genistein treatments

Liuming Xie [a,b], Gang Wang [a], Jianhua Xie [a,*], XianXiang Chen [a], Jiayan Xie [a], Xiaoyi Shi [a,b], Zhibing Huang [a,b,**]

[a] *State Key Laboratory of Food Science and Technology, Nanchang University, No. 235 Nanjing East Road, Nanchang, 330047, China*
[b] *Sino-German Joint Research Institute, Nanchang University, No. 235 Nanjing East Road, Nanchang, 330047, China*

A B S T R A C T

The exopolysaccharides (EPS) produced by the edible medicinal fungus *Monascus purpureus* (EMP) become the center of growing interest due to their techno-functional properties and their numerous applications in the food industries; however, the low EPS yields limit its application. In this study, the effect of genistein supplementation on the production, rheological and antioxidant properties of EPS by *M. purpureus* and its biosynthesis mechanism were explored. The results indicated that the addition of genistein (3 g/L) generated a 110% and 59% increase in the maximum mycelial biomass and EPS yield, respectively. The genistein supplementation group (G-EMP) had higher molar percentages of Xyl and Man, and significantly decreased molecule weight and particle size of EPS, which resulted in stronger antioxidant effect and cell growth promotion. Rheological analysis showed that both EMP and G-EMP demonstrated pseudoplastic fluid behavior and G-EMP exhibited strong gel-like elastic behavior (G' > G"). Furthermore, genistein not only facilitated the production of EPS by regulating cell membrane permeability, enhancing cellular respiratory metabolism and monosaccharide precursor synthesis pathways, and enhancing antioxidant enzyme activity to reduce oxidative stress damage, but also affected the composition of the monosaccharides by increasing enzyme activity in the underlying synthesis pathways. These findings expand the application of *M. purpureus* resources and provide a paradigm for future study of the structural and functional characteristics of EPS.

1. Introduction

Exopolysaccharides (EPS) are by-products of the microbial metabolism, which have attracted attention in recent years owing to their various potential applications (Bhawal et al., 2021; Wang et al., 2021; Wang et al., 2020, 2021a). EPS are non-toxic, biodegradable, and biocompatible compounds, mainly including carbohydrates, but also phospholipids, deoxyribonucleic acids, proteins, and non-carbohydrates (Hou et al., 2020; Nwodo et al., 2012; Peng et al., 2015). Microbial polysaccharides have several beneficial attributes and unique structures. Therefore, they are widely employed as food additives, bioflocculants, biosorbents, drug delivery agents, and pharmaceutical materials (Chen et al., 2022a; Liu et al., 2020; Silva et al., 2019).

Monascus purpureus is a medicinal fungus with a long history of use that can release EPS to maintain its homeostasis and prevent external disturbances (Xie et al., 2022). However, the low yield of EPS production is a serious limitation to the applications of EPS. Submerged fermentation (SmF) of mycelium is a fast and easy approach to acquire fungal biomass and produce polysaccharides (Hu et al., 2022). The main factors that influence EPS synthesis in filamentous fungi are medium composition, incubation temperature, incubation time, and addition of exogenous chemicals (Xu et al., 2019).

Additives such as surfactants, vegetable oils, ions, and fatty acids have significant effects on the production of EPS (Xu et al., 2019; Ye et al., 2015). For example, the addition of Tween 80 to the *Schizophyllum commune* fermentation broth increased EPS production to 3.77 g/L by enhancing cell viability and mycelial dispersion and length (Meng et al., 2021). The supplementation of *Coix lacryma* oil in the *Ganoderma lucidum* deep culture solution directly affected the biosynthesis of α-phosphoglucomutase and phosphoglucose isomerase, thus increasing EPS

---

production (Yang et al., 2013). Additionally, Tween 80 has improved the efficiency of fungal nutrient utilization, maintained the integrity of mycelial spheres, and improved cell membrane permeability in the SmF of fungal extracellular polysaccharides (Zhang and Cheung, 2011). Flavonoids have been shown to effectively reduce orangiferin in *M. purpureus*. Rutin had no significant effect on mycelial growth but effectively reduced the citrinin produced by *Monascus aurantiacus* Li AS3.4384 (Huang et al., 2019). Previous studies have found that the addition of genistein, a flavonoid, to the SmF of *M. purpureus* alters EPS structure, thereby increasing their immunomodulatory activity (Xie et al., 2022a). However, the effects of genistein on the mycelial growth and EPS synthesis of *M. purpureus* have not been investigated, and the stimulating mechanisms is still unkonw, and need to be deeply analyzed.

In this study, we speculated the genistein can promote EPS secretion by functioning as nutrients and by modulating the cellular morphology and membrane permeability of *M. purpureus*. To test these possibilities, we conducted a comparative study of the metabolic capabilities of *M. purpureus* related to cell morphology and EPS metabolism using RNA sequencing (RNA-seq) analysis. Furthermore, the effect of genistein supplementation on the production, rheological and antioxidant properties of EPS by *M. purpureus* were also explored. Our results might substantially hasten the commercial manufacturing and utilization of *M. purpureus* EPS.

2. Materials and methods

2.1. Material and reagents

Monascus purpureus 40269 was purchased from China Industrial Culture Collection (Beijing, China). Ferrozine, 1,1-diphenyl-2-picrylhy-drazyl (DPPH), and 2,2′-azino-bis-(3-ethylbenzothiazoline-6-sulphonic acid) (ABTS) were obtained from Aladdin Reagent Co., Ltd. (Shanghai, China). Reagent kits for measuring the levels of superoxide dismutase (SOD), reduced glutathione (GSH), catalase (CAT), and bicinchoninic acid protein were kindly provided by Beyotime (China). The assay kits to detect phosphoglucomutase (pgm), glucose-6-phosphate isomerase (GPI), and mannose-6-phosphate isomerase (MPI) were was kindly provided by Shanghai Enzyme-linked Biotechnology (Shanghai, China). Hexokinase (HK) detection kit was purchased from (Beijing, China) Solarbio Life Science. All the other solutions were of analytical quality.

2.2. Culture media and conditions

Monascus purpureus 40269 was cultured according to our previously reported conditions (Xie et al., 2022). Briefly, M. purpureus 40269 was inoculated in seed culture flasks containing 3 g/L of NaNO$_3$, 30 g/L of glucose, 0.5 g/L of KCl, 0.5 g/L of MgSO$_4$•7H$_2$O, and 2 g/L of KH$_2$PO$_4$. At the same time, genistein was weighed and added to the fermentation substrate, then distilled water was added and stirred for 15min. Steri-lisation was then carried out at 121 °C for 30 min. After being fermented for 2 days at 180 rpm and 30 °C, 9 mL of culture was inoculated into 90 mL of fermentation media containing no or different concentrations of genistein (0.5, 1, 1.5, 2, 2.5, 3, 3.5, and 4 g/L), and cultured for 4 days in a rotational shaker at 30 °C and 180 rpm.

The freshly collected mycelium was evenly scattered in a clean Petri dish and photographed to observe its macroscopic morphology. Additionally, the microstructure of the mycelium of the M. purpureus 40269 was observed via scanning electron microscopy (SEM, JEOL, Japan), as previously reported (Hu et al., 2022; Liu et al., 2020).

2.3. Extraction of EPS

After culture, the fermentation broth was filtered, and the M. pur-pureus 40269 cells were separated from the filtrate by centrifugation. The mycelia were filtered, scrubbed, freeze-dried, and dried overnight at 70 °C in a hot air dryer to maintain a constant weight. The fungal growth

was expressed as dry weight per biomass (dw/L). The centrifuged su-pernatant was concentrated at 65 °C with a rotary vaporizer, and then 95% volume of ethanol was added to remove pigments, small molecules, and other magazines. The concentrates were digested with 2% (w/w) papain at 55 °C for 1 h. Then, the crude EPS were centrifuged at 10,000×g for 10 min, deproteinized by the Sevag method, and precipi-tated with four volumes of anhydrous ethanol. The precipitate was sequentially washed with acetone and anhydrous ethanol. Finally, the samples were dialyzed against distilled water under running water for 72 h and freeze-dried to obtain pure EPS. EPS produced in medium supplemented with genistein were denoted as G-EMP, whereas EPS produced in medium without genistein were denoted as EMP. Dialyzed G-EMP was powered and stored in sealed bags in a desiccator.

2.4. Molecule weight and monosaccharide composition

Molecular weight (Mw) of EMP and G-EMP were measured using the Agilent 1260 high-performance liquid chromatograph. Dextran of different Mws was used as standard, and the standard curve was generated according to the relative molecular mass and logarithm of retention time, and then the Mw of EMP and G-EMP were evaluated according to the retention time. The monosaccharide content of EPS was quantified as described previously using high-performance anion ex-change chromatography with pulsed amperometric detection (Xie et al., 2020). Briefly, 0.5 mL of 12 M concentrated sulfuric acid was added to a test tube containing 5 mg of sample. Stir magnetically for 30 min in an ice bath, added 2.5 mL of ultrapure water, and then reacted for 3 h at 105 °C in an oil bath. After the reaction was completed, it was cooled, and the reaction solution was diluted with a certain multiple. Finally, the solution was injected after filtration through 0.22 μm hydro-membranes.

2.5. Particle size (Z_{avg}), zeta-potential and rheological properties

Z_{avg} and zeta potential of EMP and G-EMP solutions (1 mg/mL) were quantified at 25 °C using the Zetasizer nanosize (ZS90, Malvern, UK).

The rheological properties of EMP and G-EMP were investigated using the ARES rheometer (TA Instruments, USA) with a 40 mm diam-eter and 1 mm gap parallel plate. The steady-state shear viscosities of the EMP and G-EMP were recorded at 25 °C as shear rate of 0.1–100 s^{-1}. A power-law model was employed to fit the obtained data:

$$\tau = K(\gamma)^n \tag{1}$$

where τ, K, (γ), and n are the shear stress (Pa), consistency coefficient (Pa•s^n), shear rate (s^{-1}) and flow behavior index, correspondingly.

The dynamic rheological characteristics of the EMP and G-EMP were carried out via rheometer in the frequency range from 0.1 to 200 rad/s at 1% strain to obtain loss modulus (G″), storage modulus (G′), and loss tangent (tanδ = G″/G′) values. The obtained data was fitted via the following power-law model.

$$G' = \lambda(\omega)^N \tag{2}$$

where G′, λ, ω, and N were denoted as the storage modulus, model constant, angular frequency and slope, correspondingly.

2.6. Antioxidant effects

DPPH radical scavenging experiments were performed on EMP and G-EMP samples using a previously described method (Zhu et al., 2021). Polysaccharide solutions at different concentrations (0, 0.5, 1, 1.5, 2, 2.5, and 3 mg/mL) were prepared in distilled water. Each poly-saccharide solution (2 mL) was mixed with 3 mL of a DPPH-methanol solution (0.1 mM), and the mixture reacted for 30 min at room tem-perature under light-proof conditions. The absorbance was measured at 517 nm using ascorbic acid (Vc) as a positive control. The DPPH free
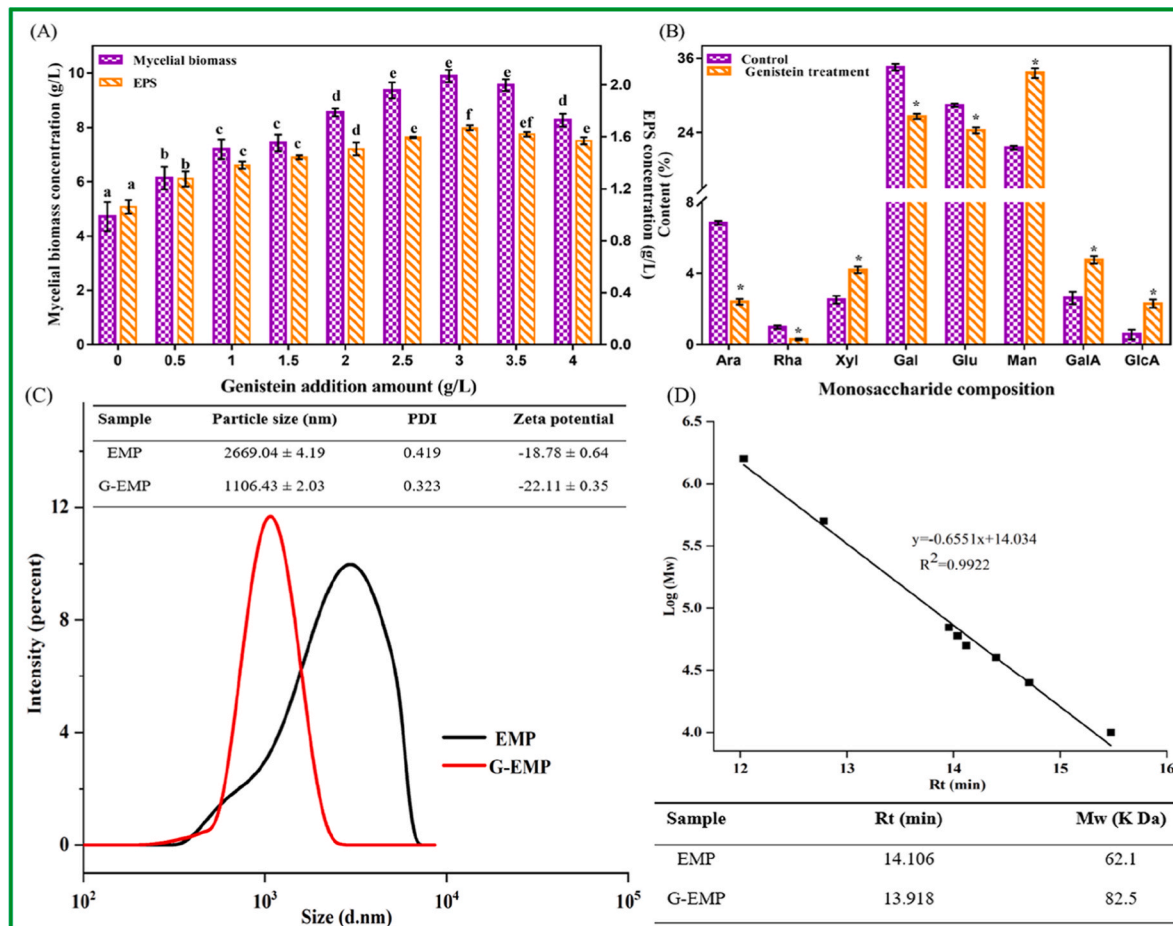
Fig. 1. Effect of genistein on *Monascus purpureus* 40269. (A) Effect of genistein on mycelial biomass and EPS yield; Effect of genistein on the monosaccharide composition (B), Zavg and zeta-potential (C), and molecular weights (D) of EPS. Different letters or '*' denote significant differences ($p < 0.05$). Data are represented as mean ± SD (n = 3).

radical removal effect was estimated as follows:

$$\text{DPPH removal effect (\%)} = \frac{A_0 - A_1 + A_2}{A_0} \times 100\% \quad (3)$$

where A_0 is the absorbance of distilled water, A_1 is the absorbance of polysaccharide samples, and A_2 is the absorbance of polysaccharide samples and distilled water.

EMP and G-EMP solutions were prepared at various concentrations (0–3 mg/mL) according to Xie et al. (2022b). The polysaccharide solutions were supplemented with 1 mL of salicylic acid (0.6 mM), 1 mL of $FeSO_4$ (1.5 mM), and 1 mL of H_2O_2 (0.1%). The mixture was heated in a water bath at 37 °C for 30 min with continuous shaking. The absorbance of the reaction mixture was measured at 510 nm to calculate the hydroxyl removal effect.

$$\text{Hydroxyl removal effect (\%)} = \frac{A_0 - A_1 + A_2}{A_0} \times 100\% \quad (4)$$

where A_0 is the absorbance of distilled water, A_1 is the absorbance of polysaccharide samples, and A_2 is the absorbance of polysaccharide samples and distilled water.

Briefly, EMP and G-EMP solutions (0, 0.5, 1, 1.5, 2, 2.5, and 3 mg/mL) were added to ABTS (4 mL). The mixture was shaken vigorously, and its absorption was measured at 734 nm using Vc as a positive control (Cao et al., 2020).

$$\text{ABTS removal effect (\%)} = \frac{A_0 - A_1 + A_2}{A_0} \times 100\% \quad (5)$$

where A_0 is the absorbance of ABTS solution and distilled water, A_1 is the absorbance of polysaccharide samples, and A_2 is the absorbance of polysaccharide samples and distilled water.

2.7. Cytotoxicity assessment

The effect of EMP and G-EMP on cell viability was assessed basing on the CCK-8 method (Fang et al., 2022). IEC-6 cellsand L-02 cellswere purchased from Chinese Academy of Sciences and Keegan Biotechnology Cell Bank, respectively. IEC-6 cells were generated in DMEM in activated fetal bovine serum (FBS) containing 10% (v/v), and L-02 cells were sustained in RPMI-1640 with the addition of 16% FBS. All cells were exposed to a hygrometry atmosphere of 5% CO_2 at 37 °C.

Briefly, IEC-6 cells (2×10^4 cells/well, 100 μL) and L-02 cells (2×10^4 cells/well, 100 μL) were separately seeded on 96-well plates for 24 h. Then, various concentrations (0–1000 μg/mL) of EMP and G-EMP were added to pretreat IEC-6 cells and LO-2 cells. Subsequent to incubation, the absorbance of the cell samples was monitored at 450 nm using a Thermo Scientific Varioskan Flash (Thermo, USA). Wells without cells were used as blanks. Growth inhibition rate was calculated as follows:

$$\text{Cell viability (\%)} = \frac{A_{450\ treated} - A_{450\ blank}}{A_{450\ control} - A_{450\ blank}} \times 100\% \quad (6)$$

2.8. Transcriptome analysis

The mycelium of M. purpureus fermented for 4 days in the treatment
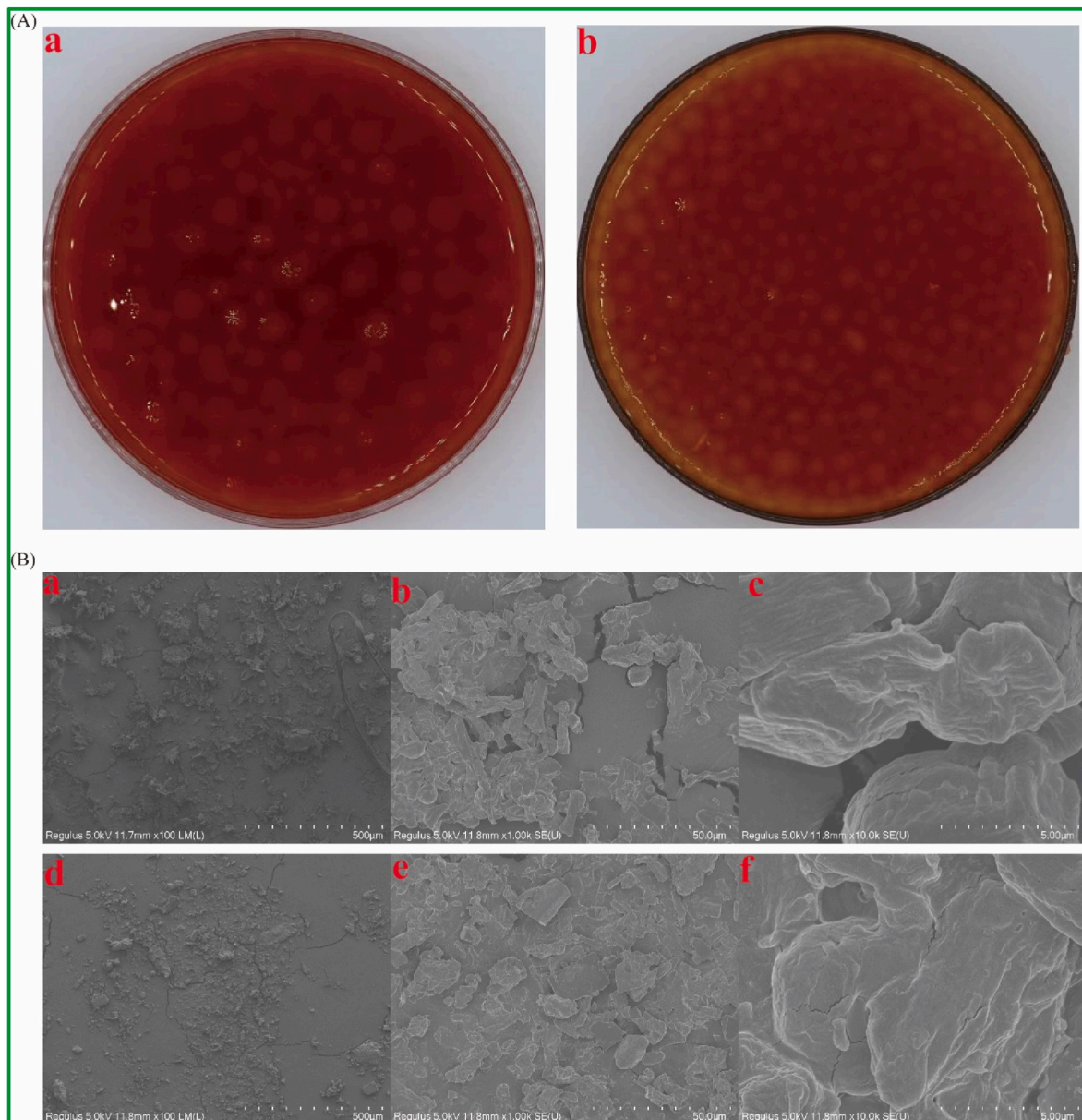
Fig. 2. (A) Macroscopic morphology of *M. purpureus* mycelium, where a is the control and b is the genistein-treated group. (B) SEM images of mycelium from left to right at magnifications of 100 × , 1000 × , and 10000 × , respectively, where a−c are control samples and d−f are genistein-treated samples.

(G-EMP) and control (EMP) groups were rapidly frozen in liquid nitrogen for approximately 5 min and immediately refrigerated at −80 °C. These samples were then subjected to RNA extraction, cDNA construction, and RNA sequencing analysis (Shanghai Personal Biotechnology, Shanghai, China). Illumina HiSeq raw sequencing contained low quality data. R statistical software was used to determine the differentially expressed genes (DEGs) between EMP and G-EMP samples. The criteria for screening DEGs were p-adjust < 0.05 and |log 2 FC| ≥ 1. To count and differentiate DEGs, Blast2GO software was used for gene ontology (GO) annotation in terms of cellular composition (CC), biological process (BP), and molecular function (MF). KOBAS software was used to analyze metabolic pathways depending on the degree of Kyoto Encyclopedia of Genes and Genomes (KEGG) enrichment. To ensure the accuracies of the results, the Benjamini-Hochberg methods were adopted to verify p-values.

2.9. Enzymatic activity assays

Monascus purpureus mycelium (50 mg) was grinded in liquid nitrogen, rinsed with buffer, transferred to a centrifuge tube for homogenization through a homogenizer, and centrifuged at 12,000 g for 15 min. The enzymatic activity of the obtained supernatant was assayed using detection kits.

2.10. Date analysis

Data were expressed as the mean ± SD of three replicates. All statistical analyses were performed using SPSS 19.0 (IBM, USA). Differences were considered statistically significant at p < 0.05.
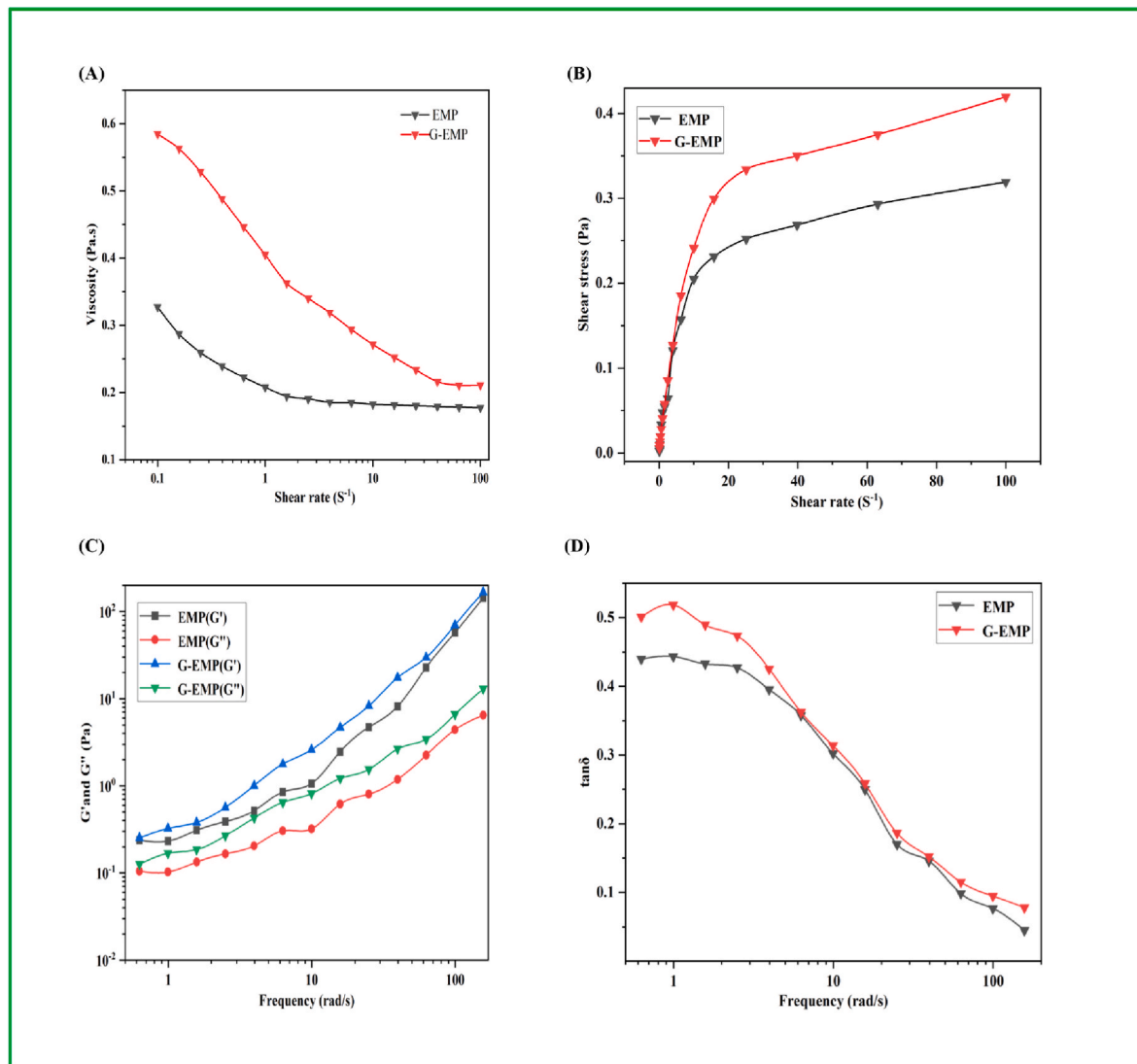
Fig. 3. Rheological properties of EMP and G-EMP gels: (A) viscosity, (B) shear stress, (C) G′ and G″ with angular frequency, and (D) tanδ with angular frequency.

3. Results and discussion

3.1. Effect of genistein on the mycelial biomass and EPS production of M. purpureus 40269

The effect of genistein dosage on the mycelial growth and EPS production of *M. purpureus* 40269 was investigated by adding different concentrations of genistein. The mycelial biomass of *M. purpureus* 40269 increased along with the genistein concentration, reaching a peak value of 9.89 g/L by adding 3 g/L of genistein, which was 2.10 times higher than that of the control (4.71 g/L) (Fig. 1A). Genistein concentrations >3 g/L in the fermentation broth decreased the mycelial biomass. Similarly, EPS yield reached a maximum of 1.67 g/L by adding 3 g/L of genistein, which was 1.59 times higher than that of the control (1.06 g/ L). The addition of external substances to SmF has been extensively reported to promote polysaccharide synthesis (Hu et al., 2022a). For example, the EPS yields of *Grifola frondosa* SmF were improved by the addition of soybean and olive oils; however, reduced EPS yields were observed with the supplementation of sunflower seed oils and safflower (Hsieh et al., 2008). Flavonol flavonoids can stimulate or suppress the mycelial growth of *Glomus* and *Gigaspora* (Scervino et al., 2005). Interestingly, the genistein concentration in the fermentation solution decreased substantially at the end of the fermentation (data not shown).

Genistein might be assimilated and used as a carbon source, thereby enhancing the metabolism of *M. purpureus* 40269.

3.2. Morphological characteristics

During shake flask fermentation, genistein significantly affected cell morphology. In the control group, the mycelium of *M. purpureus* 40269 was predominately ball-shaped or globular and rough, whereas it was fine and smooth in the treatment group, suggesting that genistein can alter the morphology of the mycelium (Fig. 2A). The structural form of the mycelium affected its oxygen uptake and nutrient transport. For example, dense mycelia with relatively large dimensions usually suffer from nutrient and oxygen restrictions within the particle core. In this experiment, it was found that the mycelial spheres were significantly reduced by the addition of genistein, which may be related to their high yield, as smaller spheres promote nutrient transport, similar to the results found in Hu et al. (2022). Upon exceeding the limiting diameter, the dispersion of oxygen in the mycelial spherical core is blocked, thereby hindering the metabolism of microorganisms (Bol et al., 2021). Consequently, the loose and small mycelium spheres observed in the genistein-treated group can facilitate the efficient transport and consumption of nutrients, leading to a remarkable enhancement of EPS and biomass yields.

The influence of genistein on the microscopic structure of mycelia was determined using SEM images. The control group showed flaky mycelia with thick and rough surfaces and uneven growth (Fig. 2B). In contrast, the treatment group showed fine mycelia with smooth and complete surfaces. These results suggested that genistein facilitated the mycelial growth and EPS synthesis by changing the mycelial morphology. Flavonoids can enhance the membrane penetration of mycelium cells, as the thickening of the cell wall is responsible for the increased permeability of the cell membrane (Jiang et al., 2022). Accordingly, we hypothesized that genistein enhances the permeability of cell membranes, thereby promoting the uptake and consumption of fermentation substrates. Consequently, the vigorous metabolism of *M. purpureus* 40269 might promote mycelial growth and EPS synthesis. Alternatively, the thickness of the cell wall might be increased by enhancing the biosynthesis of cell wall polysaccharides.

3.3. Mw and monosaccharide composition

To further confirm whether genistein merely stimulated EPS production in or altered EPS metabolic processes, the *Mw* and monosaccharide composition of the samples were examined. The *Mw* of EPS decreased from 82.5 kDa to 62.1 when *M. purpureus* was pretreated with genistein (Fig. 1D). EPS of both control and treatment groups were composed of eight monosaccharide units, including arabinose (Ara), xylose (Xyl), mannose (Man), glucose (Glc), galactose (Gal), rhamnose (Rha), glucuronic acid (GlcA), and galacturonic acid (GalA) (Fig. 1B). The main sugar skeleton of both EPS groups contained Glc, Gal, and Man. The addition of genistein remarkably increased the proportion of Man, whereas the proportions of Glc and Gal were significantly reduced. These findings suggested that genistein supplementation not only promoted EPS production and mycelial growth but also altered the metabolic processes related to EPS synthesis. Based on previous studies on EPS synthesis, two mechanisms might explain our findings: 1) genistein might facilitate the movement of DDP-Glc towards GDP-Man in the NDP-sugar synthetic phase, and/or 2) *M. purpureus* 40269 might preferably use UDP-Gal and GDP-Man rather than UDP-Glc for the synthesis of repetitive EPS units (Cui et al., 2016; Hu et al., 2022). Therefore, it is necessary to study it further in depth.

3.4. Effect of genistein on Z_{avg}, zeta-potential and rheological properties of EPS

A significant drop in Z_{avg} of EPS was recorded after genistein treatment (Fig. 1C). The Z_{avg} wavelength of EMP was dramatically diminished from 2669.04 ± 4.19 nm to 1106.43 ± 2.03 nm (p < 0.05), in agreement with the variation of Mw. The results indicated that the addition of genistein to the medium could be an effective method to obtain the reduced Mw t of EPS.

In Fig. 1C, the zeta-potential of EMP and G-EMP were further calculated. The zeta-potentials of EMP and G-EMP were −18.78 ± 0.64 and −22.11 ± 0.35 mV, respectively, implying that the EMPs particles had negative charge and the negative charge of the EPS was attributed to the existence of uronic acid, which was consistent with the findings of the physicochemical characteristics of EMPs. The relatively higher the absolute level of zeta potential of the sample, the greater the stability of the system, while the lower the absolute level of zeta potential, the weaker the system (Agbenorhevi et al., 2011). The results showed that the G-EMP solution was more stable than the EMP, however, the rheological behavior of the specific solution required further study.

Solution behavior was another critical parameter of EPS, which was employed to demonstrate any structural and conformational changes. The steady-state shear results for EMP and G-EMP were shown in Fig. 3A and B. The apparent viscosity of EMPs were decreased sharply with the enlarging shear fence. The viscosity of G-EMP solution was stronger than that of EMP at the same concentration, indicating that the addition of genistein significantly increased the apparent viscosity of EMP solution.

Table 1
Power law parameters of rheological properties of EPM and G-EMP gels.

Sample	Stress versus shear rate			G′ versus angular frequency		
	K	n	R^2	λ	N	R^2
EMP	0.067 ± 0.009	0.366 ± 0.037	0.96	0.006 ± 0.000	2.010 ± 0.017	0.99
G-EMP	0.079 ± 0.011*	0.391 ± 0.009*	0.97	0.017 ± 0.003*	1.822 ± 0.041*	0.99

Data represent mean ± SD (n = 3). '*' denote significant differences (p < 0.05).

The parameters of the power-law model for EMP and G-EMP solutions were illustrated in Table 1. The R^2 values for all EMPs solutions were higher than 0.9, suggesting that the power-law model can be employed to describe the flow behavior of EMP solutions after genistein treatment. When n = 1, the fluid was the desirable fluid (Newtonian fluid); when the value of n was more than 1, the fluid was a non-Newtonian fluid and displayed shear-thickening behavior. When the value of n was lower than 1, the fluid was also a non-Newtonian fluid (pseudoplastic fluid) and showed shear thinning behavior. Fluids with higher pseudoplasticity had relatively low n levels. A previous work has reported that polysaccharide solutions are mostly pseudoplastic liquids (Yuan et al., 2020). In our study, the n-values of the EMPs solutions were all lower than 1, which indicated that the EMPs solutions were pseudoplastic fluids with very low viscosity. The n-value was increased after the treatment with genistein, suggesting that the apparent viscosity of the EPS solution was obviously enhanced. The different Mw and monosaccharide composition ratios of EMPs may be the main reason for the different viscosity of EPS (Hu et al., 2022b).

The dynamic modulus values in EMPs were all enlarged with the increase of frequency and showed a clear frequency dependent (Fig. 3C). G′ was always higher than G″ in the measurement frequency range, indicating that EMPs gels were solid-like gels. In general, G′ and G″ respectively reflected the elasticity and viscosity of the given materials. The G′ and G″ values of genistein treated EMP were greater than those of the native EMP system, demonstrating that genistein treatment could significantly improve the viscoelasticity of the EMP system. Similar behavior was observed on the Sargassum pallidum polysaccharides (Yuan et al., 2020). The behavior of these changes suggested that the ability of EMP in water to form entangled network was enhanced after treatment of the M. purpureus 40269 with the genistein. This might also be due to the fact that more intermolecular regions could participate in noncovalent linkage under the treatment of genistein, leading to the formation of a stronger three-dimensional network of polysaccharides (Ding et al., 2021).

The loss tangent (tanδ) serves to represent the dynamic viscoelastic behavior of the fluid and is the proportion of G″/G'. Typically, tanδ <1 indicates elastic behavior and tanδ >1 indicates viscous behavior. The tanδ values for all EMPs samples were universally below 1 (Fig. 3D), supporting that both the native and genistein treated EMP/water systems exhibited elastic behavior throughout the frequency range (Yuan et al., 2020). However, the tanδ of EMP and G-EMP were close to 0.5 in the low frequency range (0.01–1 Hz), which inferred the weak formation of gel structure between dilute solution and elastic gel (Ding et al., 2021). Interestingly, Strong gels were obtained for EMP and G-EMP with the increase in frequency where tanδ nearly equal to 0.05.

The power-law model was adopted to examine the scanned data of EMPs gels, and the power-law parameters of the rheological properties of EMPs gels were detailed in Table 1. The coefficients for the models were all over 0.99, which were in good agreement with the experimental data. A higher λ value of the sample indicated a stronger gel network (Chen et al., 2022b). The λ values for the G-EMP group was greater than that for the EMP group, suggesting stronger gel networks. Based on the analysis of all the above rheological results, G-EMP may be more suitable for use in gel food products including jellies and certain food additives such as thickeners and gelling agents.
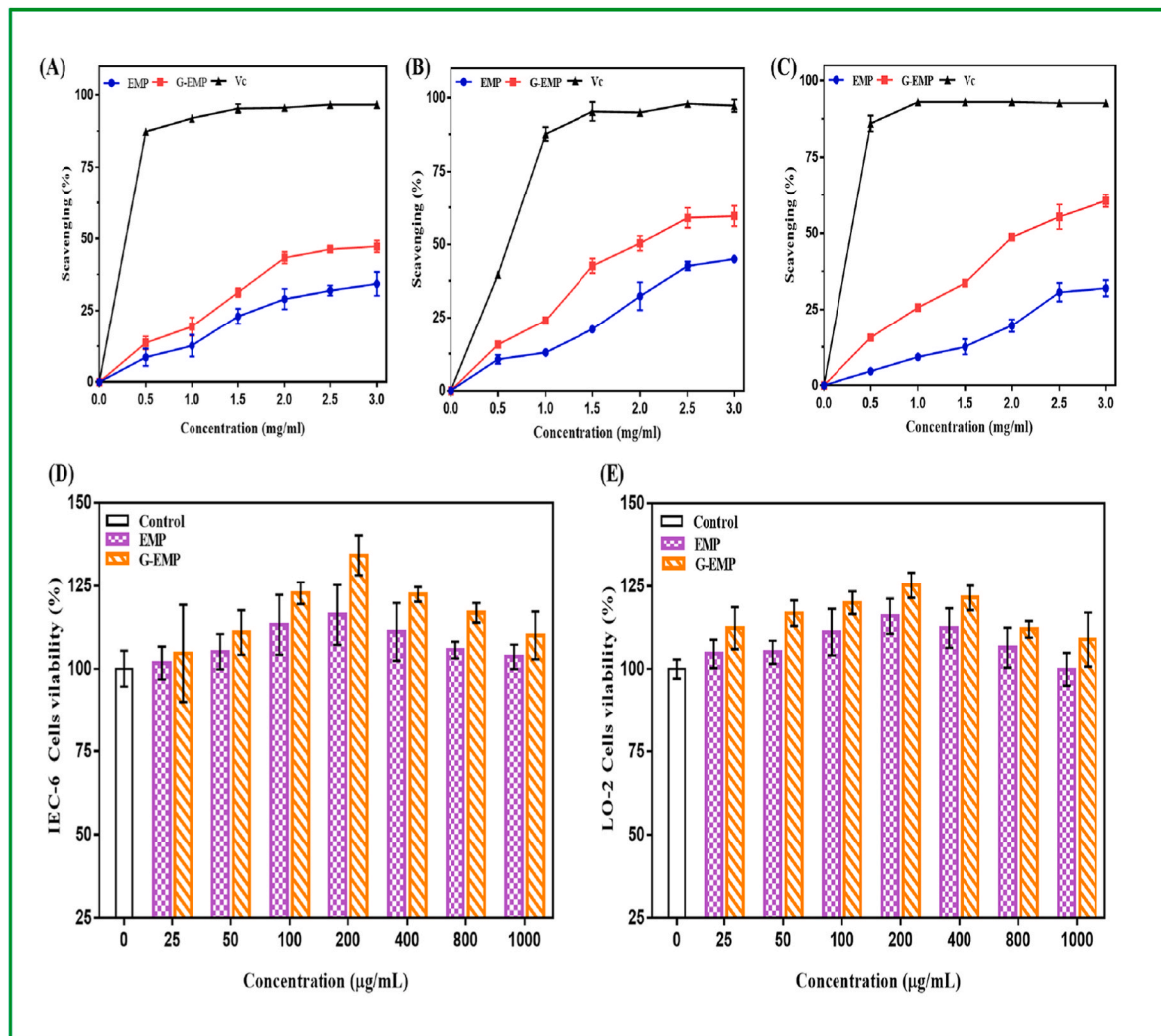
Fig. 4. Antioxidant effects of EMP and G-EMP: scavenging effects of (A) DPPH, (B) ●OH, and (C) ABTS radicals; and cell viability of EMP and G-EMP on (D) IEC-6 cells and (E) LO-2 cells. Data are represented as mean ± SD (n = 6).

3.5. Antioxidant effects

DPPH radical removal was the original method used to test and develop natural antioxidants (Wang et al., 2021b). G-EMP in the concentration range of 0–3 mg/mL presented a scavenging effect on DPPH radicals in a dose-dependent manner. The DPPH radical removal of G-EMP was 47.33% at 3 mg/mL (Fig. 4A). Our results indicated that G-EMP possessed significant scavenging effects on DPPH radicals and that the addition of genistein further boosted the remotion of DPPH radicals, particularly at high doses. The antioxidant effects of EPS are associated with their uronic acid content, *Mw*, substituents, and glycosidic bonds (Cui et al., 2016). The addition of genistein altered the structure of EPS, causing variations in the uronic acid content (Xie et al., 2022a) and *Mw*. Hence, the correlation between antioxidant activation and EPS structure requires further investigation.

●OH radicals can break DNA strands, leading to cytotoxicity, mutations, carcinogenesis, or other biological effects (Ji et al., 2020; Xie et al., 2020). The ability of EPS to scavenge ●OH was determined by detecting the oxidative damage to sugar moieties via ●OH. The clearance of EPS samples was related to the increase in EPS concentration (Fig. 4B). The G-EMP removal of ●OH radicals was 59.67% at 3 mg/mL, which was significantly higher than that of EMP, but lower than that of the *Vc* group. Compared to EMP (63%), G-EMP exhibited higher total sugar content (76%) and higher antioxidant activation of the samples

(Hasheminya and Dehghannya, 2020). Additionally, the antioxidant effect was governed by the *Mw* and monosaccharide composition of EPS. EPS with low *Mw* possess more reducing hydroxyl termini to receive and abolish foreign radicals than those with high *Mw* (Wang et al., 2021b). The *Mw* of EPS in the genistein-treated group (62.1 kDa) was lower than that in the blank group (82.5 kDa). However, the molecules involved in the removal of free radicals need to be further investigated owing to the uncertainty of the complex role of the elements contributing to the antioxidant effect of EPS.

ABTS assay is extensively employed to evaluate the antioxidant power of hydrophilic and lipophilic compounds, as it reflects the ability of antioxidants to donate hydrogen (Sirin and Aslim, 2021). Both EMP and G-EMP samples exhibited ABTS scavenging effects, and their removal rates were typically dose-dependent and lower than that of the control group (Fig. 4C). The scavenging effect of ABTS by EMP and G-EMP at 3 mg/mL was 32.01% and 58.93%, respectively. Both EMP and G-EMP exhibited good antioxidant effects and that the addition of genistein promoted the removal of ABTS radicals. The antioxidant effect of EPS is closely related to its high mannose ratio, rough surface morphology, polyanionic functions (amino, hydroxyl, and carboxyl groups), and amorphous structure (Sirin and Aslim, 2021). After genistein treatment, the percentage of rhamnose in EPS increased significantly from 21% to 34% (Fig. 1B). Our previous SEM assay demonstrated that G-EMP had more voids on its surface than EMP (Xie
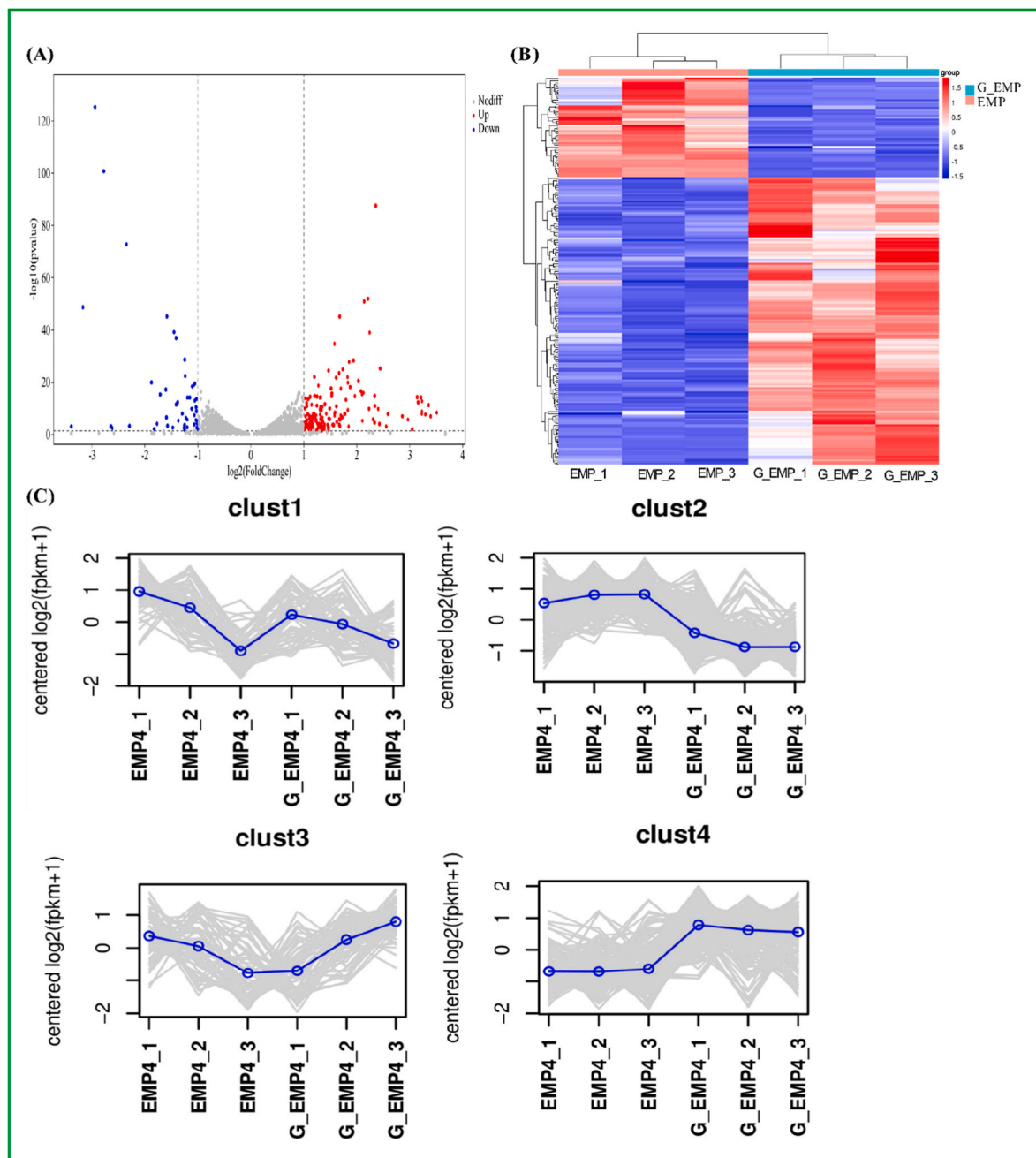
Fig. 5. (A) Volcano plots, (B) cluster heat maps, and (C) trend analysis of DEGs in the EMP and G-EMP groups.

et al., 2022a), which enlarged its exposure area to radicals and enhanced its removal efficiency (Sirin and Aslim, 2021). Furthermore, the solubility of EPS increased after genistein treatment, which may have increased antioxidant activation, whereby a higher solubility is appropriate for the efficient delivery of the active ingredient (Hasheminya and Dehghannya, 2020). Therefore, EPS treated with genistein scavenged free radicals more effectively than those without genistein. Therefore, the genistein in this study may not only increase the synthesis of EPS, but also impart improved antioxidant activity.

3.6. Cytotoxicity assessment

Some EPSs have beneficial properties in terms of antioxidant effect and non-cytotoxicity, which caught a lot of interests from the researchers and food industries (Chen et al., 2022b). The cytotoxic effects of eight various concentrations (25, 50, 100, 200, 400, 800, 1000

µg/mL) of EMP and G-EMP on IEC-6 cells and LO-2 cells were presented in Fig. 4D and E, respectively. Both EMP and G-EMP at all concentrations had no acute toxic effect on IEC-6 cells and LO-2 cells, and even G-EMP had a stronger cell growth-promoting effect than EMP.

3.7. RNA sequencing

We used RNA-seq technology to analyze the response mechanism of genistein related to EPS synthesis. A total of 199 DEGs between the EMP and G-EMP groups were screened using |log2(fold-change)| ≥ 1 and false discovery rate (FDR) values < 0.05 as thresholds. Among them, 148 DEGs were upregulated and 51 DEGs were downregulated. Visualizations of the 199 DEGs in the volcano diagram are shown in Fig. 5A. Clustering analysis and commercialization of divergent expression profiles using the heatmap package showed that DEGs were consistent between replicates and that the variation between groups was significant
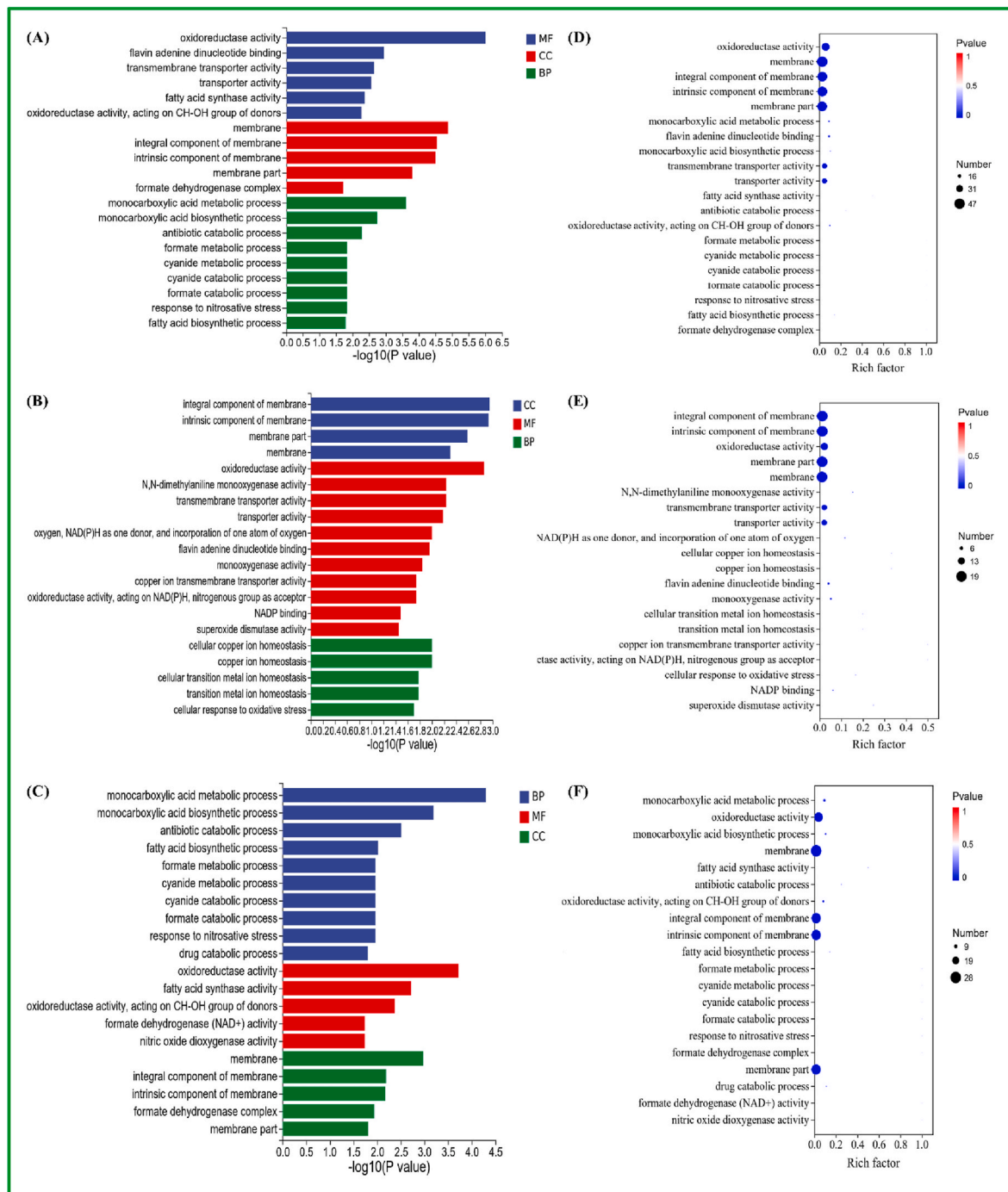
Fig. 6. (A) GO function classification of total, (B) upregulated, and (C) downregulated DEGs. (D) Significant plots of enrichment of the top 20 GO terms of total, (E) upregulated, and (F) downregulated DEGs.

(Fig. 5B). Based on the variation in gene expression profiles, four clustered line diagrams were established, one of which was a stable upregulated expression profile, suggesting that the EPS synthesis-related gene cluster (sub_cluster_4) was upregulated (Fig. 5C).

3.8. GO function analysis

GO enrichment analysis was performed across all DEGs to better visualize the feature clouds and bio-chemical routes. DEGs were predominantly clustered in cellular processes, cell membranes, metabolic processes, binding activities, and cell membrane components (Fig. 6A). In addition, the enrichment analysis with R software using FDR correction for p- and q-values ≤ 0.05 revealed that the functions were focused on membranes, membrane parts, integral and intrinsic components of membranes, oxidoreductase activity, transporter activity, and transmembrane transporter activity (Fig. 6D). These results tentatively demonstrated that genistein supplementation altered the metabolism of *M. purpureus* 40269 and/or the symmetry and properties of cell membranes and elevated cell metabolism. This also corroborated the analysis of the results of mycelium SEM.

Upregulated (148) and downregulated (51) genes were filtered to analyze the results of the functional enrichment by establishing q-value < 0.05 and |log 2 FC| ≥ 1 as thresholds to determine significant differences in DEGs. Among them, 38 and 13 remarkably upregulated
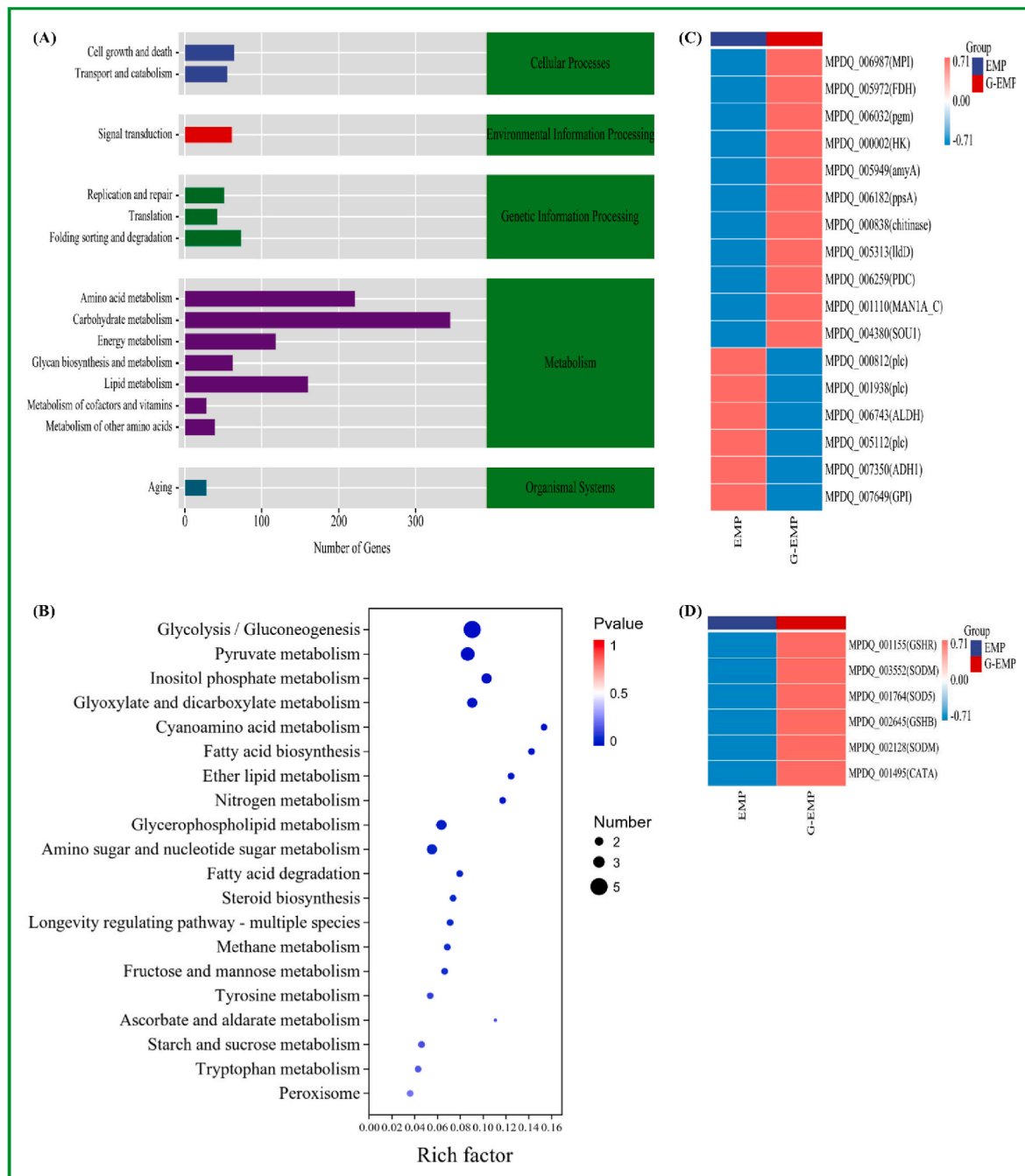
Fig. 7. (A) KEGG annotation. (B) Significant variation in KEGG functional enrichment analysis. (C) Heat map analysis of the effect of genistein on some key significant DEGs involved in EPS synthesis in the carbohydrate metabolism pathway. (D) Heat map analysis of the effect of genistein on some key significant DEGs involved in oxidative stress.

genes were associated with cell membrane metabolism and oxidoreductase activity, respectively (Fig. 6B). Nonetheless, 28 and 23 dramatically downregulated DEGs were associated with cell membrane metabolism and oxidoreductase activity, respectively (Fig. 6C). The primary 20 functionalities of the remarkably upregulated DEGs were associated with membrane (19), oxidoreductase (13), and transporter (20) (Fig. 6E). In contrast, only 12 functions were dramatically enriched by downregulated DEGs, which were predominantly associated with integral components of the membrane (25), oxidoreductase (23), and monocarboxylic acid metabolism (6) (Fig. 6F).

The correlations among these functions can be visualized in directed acyclic graphs (DAGs) via the visual GO enrichment analysis. Regarding BP (Fig. S1A), the enrichment was predominantly located in the monocarboxylic acid metabolic processes (GO:0032787), namely the chemical reactions and pathways involving monocarboxylic acids and any organic acid containing one carboxyl (COOH) or anion (COO-) group. The child functions of this process participate in the metabolism of uronic acids, fatty acids, phenolic compounds, and foreign substances, indicating that the metabolism of cellular organic substances has significant differences between the treated and control groups and that genistein may influence the metabolism.

CC was predominantly concentrated in the (GO:0016020) membrane with its downstream branches, including (GO:0031224 and GO:0016021) intramembrane components (Fig. S1B). The (GO:0016021) intramembrane component and dominant enrichment of membranes consist of the organelle, extracellular, and plasma

membranes; cytochrome *o* ubiquitin oxidase complexes; transmembrane components of membranes; and transmembrane transporter complexes. These results showed that genistein supplementation not only had significant effects on membrane transport but also promoted the biological reactions of membrane-associated complexes and cell walls.

MF was mainly enriched in (GO:0016491) oxidoreductase activity, which belongs to the sub-branch of (GO:0003824) catalytic activity (Fig. S1C). Oxidoreductase activity acts on paired donors to reduce or incorporate molecular oxygen (GO:0016705). The oxidoreductase activity included α-hydroxylase, electron transfer, monooxygenase, and NADPH-adrenergic reductase activities, suggesting that genistein had a significant effect on oxidative reduction. DAG analysis of DEGs showed that genistein supplementation affected cellular fatty acid synthesis and metabolism, formate dehydrogenase, nitric oxide dioxygenase, membrane synthesis, flavin adenine dinucleotide binding, and transmembrane transport. Nevertheless, the specific conversion of genistein needs further study.

Microorganisms can fuse the rings of flavonoid skeletons and mediate further reduction, decarboxylation, demethylation, and dehydroxylation reactions. The flavonoid A ring can be metabolized to short-chain fatty acids, which are substrates for energy metabolism (Feng et al., 2018). Coconi-Linares et al. (2015) revealed that the co-expression of oxidoreductase promoted the breakdown of phenolic compounds. In our previous study, we found that the utilization of genistein by *M. purpureus* was as high as 74% (data not shown). Together with the GO analysis in this study, we have shown that the fluidity of the cell membrane led to the accumulation genistein in the cells. Genistein was broken down inside the cells and their by-products promoted fatty acid β-oxidation and acetyl-CoA production, which elevated the cellular metabolic levels. Simultaneously, the intracellular pressure raised as genistein entered the cell and underwent metabolism, thereby changing the intracellular environment. In response to the increased pressure and to maintain the integrity of protoplasts, mycelial cells actively increased the strength of cell walls (Peng et al., 2020). The increased strength also induced the stretching of cell membranes, increasing their permeability and facilitating the passage of genistein into the cells, thus allowing more EPS across the periplasm.

3.9. KEGG function analysis

All DEGs were classified by KEGG, and most of them participated in cellular processes, organismal systems, genetic information processing, environmental information processing, and metabolic pathways (Fig. 7A). DEGs were enriched across 38 pathways. In addition to energy and carbon metabolism pathways, the top 20 pathways that were significantly enriched mainly belonged to lipid metabolism, including ether lipid metabolism, glycerophospholipid metabolism, and fatty acid degradation. Hence, the following analysis was conducted to validate the above results by focusing on the DEGs associated with polysaccharide synthesis and lipid metabolism.

DEGs were engaged in ten subclasses of carbohydrate metabolism, of which five were significantly enriched: glycolysis/gluconeogenesis, pyruvate metabolism, inositol phosphate metabolism, glyoxylate and dicarboxylate metabolism, and amino sugar and nucleotide sugar metabolism ($p < 0.05$) (Fig. 7B). The gene encoding HK (an enzyme that catalyzes the phosphorylation of hexose) was significantly upregulated in carbohydrate metabolism, as HK catalyzes the first reaction and rate-limiting step of the glycolytic pathway (Fig. 7C). HK can catalyze the production of D-fructose 6-phosphate and D-rhamnose 6-phosphate from D-fructose and D-rhamnose, respectively.

GPI is a multifunctional cytoplasmic enzyme that converts D-fructose to UDP-glucose, which in turn undergoes several transformations (Liu et al., 2021). Pgm belongs to the family of hexose phosphate metastases and is widespread in microorganisms, where its main function is to catalyze the interconversion of D-glucose 1-phosphate and D-glucose 6-phosphate and to keep them in dynamic balance (Chauton et al.,

Table 2
Enrichment analysis of DEGs related to lipid metabolism.

Pathway ID	Pathway Name	Level 1	Level 2	Candidate Gene Num
ko00071	Fatty acid degradation	Metabolism	Lipid metabolism	25
ko00564	Glycerophospholipid metabolism	Metabolism	Lipid metabolism	25
ko00100	Steroid biosynthesis	Metabolism	Lipid metabolism	27
ko00561	Glycerolipid metabolism	Metabolism	Lipid metabolism	31
ko00380	Tryptophan metabolism	Metabolism	Amino acid metabolism	38
ko01040	Biosynthesis of unsaturated fatty acids	Metabolism	Lipid metabolism	38
ko00600	Sphingolipid metabolism	Metabolism	Lipid metabolism	38
ko00061	Fatty acid biosynthesis	Metabolism	Lipid metabolism	38
ko00280	Valine, leucine and isoleucine degradation	Metabolism	Amino acid metabolism	38
ko00780	Biotin metabolism	Metabolism	Metabolism of cofactors and vitamins	9
ko00592	alpha-Linolenic acid metabolism	Metabolism	Lipid metabolism	5
ko00062	Fatty acid elongation	Metabolism	Lipid metabolism	5
ko00590	Arachidonic acid metabolism	Metabolism	Lipid metabolism	5
ko00650	Butanoate metabolism	Metabolism	Carbohydrate metabolism	21
ko04146	Peroxisome	Cellular Processes	Transport and catabolism	55
ko00310	Lysine degradation	Metabolism	Amino acid metabolism	30
ko00010	Glycolysis/Gluconeogenesis	Metabolism	Carbohydrate metabolism	55
ko00051	Fructose and mannose metabolism	Metabolism	Carbohydrate metabolism	30
ko00565	Ether lipid metabolism	Metabolism	Lipid metabolism	16
ko00909	Sesquiterpenoid and triterpenoid biosynthesis	Metabolism	Metabolism of terpenoids and polyketides	3
ko00511	Other glycan degradation	Metabolism	Glycan biosynthesis and metabolism	5
ko00053	Ascorbate and aldarate metabolism	Metabolism	Carbohydrate metabolism	5
ko00591	Linoleic acid metabolism	Metabolism	Lipid metabolism	2

2013). MPI is a metalloenzyme that reversibly catalyzes the interconversion between D-fructose 6-phosphate and D-mannose 6-phosphate and plays an important role in the synthesis of GDP-mannose (Roux et al., 2007), which is a precursor for EPS synthesis. These results also implied that the monosaccharide composition ratio of EPS was altered. The gene encoding mannosyl-oligosaccharide 1,2-alpha-mannosidase, which participates in the maturation process of N-glycans, was significantly upregulated, leading to the formation of hybrid and complex structures. These results suggested that the addition of genistein changed the monosaccharide composition and spatial structure of EPS. Noticeably, the gene encoding chitinase was significantly upregulated in amino sugar and nucleotide sugar metabolism. Chitinases are capable of catalyzing the hydrolysis of butyrin to produce vital cytoskeletal components of the fungal cell wall (Silva et al., 2019). Therefore, chitinase upregulation was in accordance with the increase in mycelial biomass in the treatment group.

The enrichment analysis of DEGs showed that the lipid metabolism

Table 3
Genes with significant up-regulation of cytochrome P450 enzymes.

Gene ID	Log2(G-EMP/EMP)	Definition
MPDQ_002770	2.31	cytochrome P450 monooxygenase
MPDQ_006021	3.23	cytochrome P450/NADPH-cytochrome P450 reductase
MPDQ_000745	1.34	cytochrome P450/NADPH-cytochrome P450 reductase
MPDQ_004224	1.30	cytochrome P450/NADPH-cytochrome P450 reductase
MPDQ_005018	1.43	cytochrome P450/NADPH-cytochrome P450 reductase
MPDQ_005326	1.17	cytochrome P450/NADPH-cytochrome P450 reductase
MPDQ_004599	1.69	cytochrome P450 monooxygenase
MPDQ_004778	1.75	cytochrome P450 monooxygenase
MPDQ_004878	1.50	cytochrome P450/NADPH-cytochrome P450 reductase
MPDQ_004360	1.19	cytochrome P450/NADPH-cytochrome P450 reductase
MPDQ_004807	1.37	cytochrome P450 monooxygenase
MPDQ_002319	1.10	cytochrome P450/NADPH-cytochrome P450 reductase
MPDQ_002849	1.36	cytochrome P450/NADPH-cytochrome P450 reductase

Table 4
Related DEGs involved in peroxisome fatty acid oxidation.

Gene ID	Name[a]	Log2(G-EMP/EMP)	Definition
MPDQ_006021	CYP102A	3.23	cytochrome P450/NADPH-cytochrome P450 reductase
MPDQ_000745	CYP102A	1.34	cytochrome P450/NADPH-cytochrome P450 reductase
MPDQ_004224	CYP102A	1.30	cytochrome P450/NADPH-cytochrome P450 reductase
MPDQ_005018	CYP102A	1.43	cytochrome P450/NADPH-cytochrome P450 reductase
MPDQ_005326	CYP102A	1.17	cytochrome P450/NADPH-cytochrome P450 reductase
MPDQ_004878	CYP102A	1.50	cytochrome P450/NADPH-cytochrome P450 reductase
MPDQ_004360	CYP102A	1.19	cytochrome P450/NADPH-cytochrome P450 reductase
MPDQ_002319	CYP102A	1.10	cytochrome P450/NADPH-cytochrome P450 reductase
MPDQ_002849	CYP102A	1.36	cytochrome P450/NADPH-cytochrome P450 reductase
MPDQ_002179	PDCR	1.21	peroxisomal 2,4-dienoyl-CoA reductase
MPDQ_003087	ABCD	1.09	peroxisomal long-chain fatty acid import protein
MPDQ_000343	ECH	1.08	delta3,5-Delta2,4-dienoyl-CoA isomerase
MPDQ_005629	ACOX	1.05	acyl-CoA oxidase

[a] CYP102A: cytochrome P450/NADPH-cytochrome P450 reductase; PDCR: peroxisomal 2,4-dienoyl-CoA reductase; ABCD: ATP-binding cassette, subfamily D (ALD), peroxisomal long-chain fatty acid import protein; ECH: Delta3,5-Delta2,4-dienoyl-CoA isomerase; ACOX: acyl-CoA oxidase.

included 23 pathways (Table 2), mainly related to fatty acid degradation, glycerophospholipid metabolism, and sphingolipid metabolism. In addition, 51 DEGs were selected by setting q-value < 0.05 and |log2FC| ≥ 1 as thresholds to determine significant differences in DEGs, of which 27 genes were upregulated and 34 genes were downregulated. Our results revealed that the expression levels of fatty acid β-oxidation-related genes, including acetyl-CoA hydrolase and enoyl-CoA hydratase, were remarkably elevated.

Moreover, genes encoding for cytochrome P450 enzymes were markedly upregulated (Table 3). P450 monooxygenase is known to rapidly catalyze the monooxygenation reaction of saturated fatty acids

with chain lengths between C12–C18, using the ω-oxidation pathway of fatty acid oxidation (Miura and Fulco, 1974). Other markedly upregulated DEGs may be allocated to the peroxisome pathway (Table 4). In particular, CYP102A was involved in α-oxidation; α-methylacyl-CoA racemase, acyl-CoA oxidase, sterol carrier protein 2, and acetyl-CoA acyltransferase 1 were involved in β-oxidation; and peroxisomal 2, 4-dienoyl-CoA reductase, ATP-binding cassette subfamily D, and delta 3,5-delta 2,4-dienoyl-CoA isomerase were involved in the β-oxidation of unsaturated fatty acids (Hu et al., 2022). Consequently, fatty acids entering the peroxisome were oxygenated to short-chain fatty acids, which then entered the mitochondria for β-oxidation to produce acetyl-CoA, which is subsequently involved in the citric acid cycle. The addition of genistein increased the level of fatty acid β-oxidation and acetyl-CoA available to enter the citric acid cycle, thus elevating the cell metabolic levels and biomass and EPS production.

The metabolism of xenobiotics was enriched, as seven cytochrome P450 (ko00980) genes were significantly upregulated. Generally, xenobiotics are metabolized through stage I and stage II transformations. Stage I (catabolism) breaks down large xenobiotic substances into smaller units through oxidation, reduction, and hydrolysis reactions (Hamers et al., 2008). We observed the depletion of genistein at the end of the fermentations, which demonstrated that cells utilized genistein as a carbon source that was catabolized, thus enhancing cellular metabolism and biomass and EPS production.

Cellular oxidative homeostasis relies on the dynamic equilibrium between reactive oxygen species (ROS) generation and elimination (Liu et al., 2022). Prolonged sealed fermentations can produce unfavorable substances that generate oxidative stress by inducing an excessive ROS production or a reduction in the antioxidant enzyme activity. We extracted three antioxidant-related DEGs to explore the potential mechanisms of exogenous genistein in response to ROS-induced oxidative stress and enhanced antioxidant power (Fig. 7D). Our results revealed that the gene expression of the antioxidant enzymes SOD, CAT, and GSH in *M. purpureus* 40269 was upregulated after genistein treatment; these enzymes are essential components of the antioxidant defense of fungal cells (Jiang et al., 2022). SOD is a superoxide remover that decreases the H_2O_2 and MDA damage in cells (Xie, L., Shen, M., Wang, Z., & Xie, 2021). Moreover, glutathione serves as the core and predominant non-enzymatic system that protects cells from oxidative stress (Jiang et al., 2022). In the present study, the antioxidant enzyme activity increased after genistein treatment to maintain a stable intracellular environment, thus promoting EPS synthesis.

3.10. Validation and analysis of key enzymes

To confirm the transcriptome results, seven enzymes associated with EPS synthesis and antioxidant enzymes were tested further. The comparison of the expression status of these enzymes in the EMP and G-EMP samples revealed that their expression patterns were in agreement with the trends observed in the transcriptome data (Fig. 8). These findings demonstrated the reliability of the RNA-seq data.

4. Conclusion

In summary, the addition of genistein (3 g/L) increased EPS yield to 1.67 g/L and mycelial biomass to 9.89 g/L. The supplementation of genistein resulted in finer, rounder and smoother mycelium and significantly changed the monosaccharide composition ratio, *Mw*, Zavg and zeta-potential of EPS. G-EMP exhibited stronger viscosity, greater shear thinning, and strong elastic gel-like behavior (G' > G'') compared to EMP. Meanwhile, the genistein-treated EPS samples had a stronger antioxidant capacity for the scavenging of DPPH, hydroxyl, and ABTS radicals that of the control group and no cytotoxicity. Moreover, the positive effects of genistein on EPS synthesis are reflected in the following aspects: (1) direct induction of the transcription of EPS synthesis gene clusters, (2) enhancement of the electron transfer respiratory
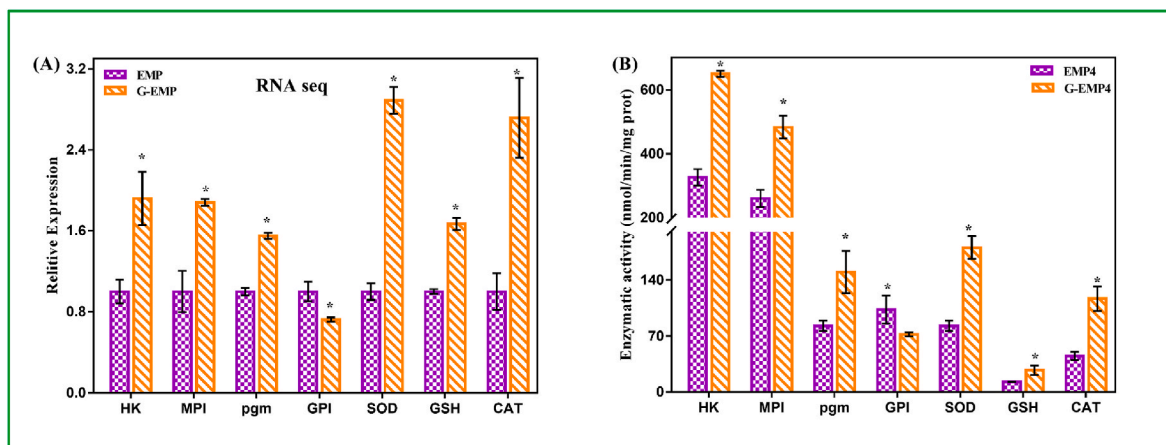
Fig. 8. (A) Expressions of some key enzymes affecting EPS synthesis (pgm, GPI, HK, MPI, SOD, GSH, and CAT). (B) Activities of some key enzymes (pgm, GPI, HK, MPI, SOD, GSH, and CAT) in *M. purpureus*. '*' denotes significant differences ($p < 0.05$). Data are represented as mean $\pm$ SD (n = 3).
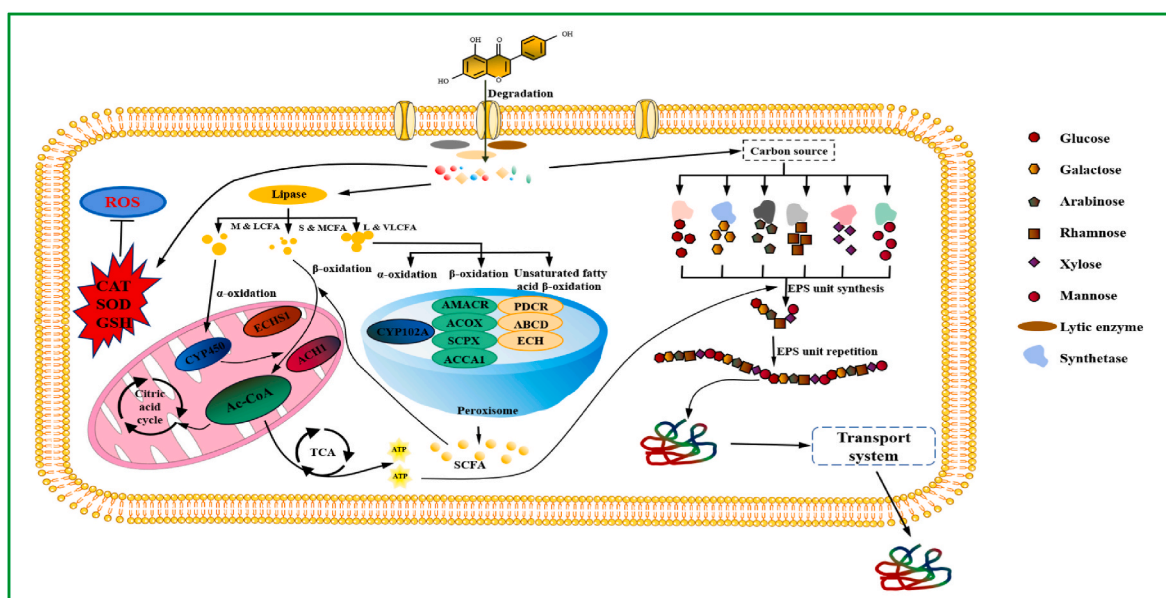

Fig. 9. Possible response mechanism of genistein to EPS production in *M. purpureus*.

chain and transporter system by strengthening fatty acid metabolism, (3) alteration of membrane permeability to facilitate EPS extrusion, and (4) enhancement of antioxidant enzyme activity to cope with the damage caused by the oxidative stress induced in prolonged fermentations (Fig. 9). Overall, this study successfully established an efficient and high-yielding EPS production with the supplement of genistein, ant its mechanism related to regulating cell membrane permeability, enhancing cellular respiratory metabolism and monosaccharide precursor synthesis pathways. Furthermore, these findings offered new ideas to further understand the mechanism of release of EPS promoted by genistein and modify its physicochemical and bioactive effects, which can greatly facilitate the application of *M. purpureus* resources.

CRediT authorship contribution statement

Liuming Xie: Conceptualization, Methodology, Formal analysis, Investigation, Writing – original draft, Data curation, Visualization. **Gang Wang:** Methodology. **Jianhua Xie:** Writing – review & editing, Conceptualization, Supervision. **XianXiang Chen:** Writing – review & editing. **Jiayan Xie:** Software. **Xiaoyi Shi:** Software. **Zhibing Huang:** Validation, Resources, Writing – review & editing, Supervision.

Declaration of competing interest

The authors declare that they have no known competing financial interests or personal relationships that could have appeared to influence the work reported in this paper.

Abbreviations

ABTS	2,2′-azino-bis-(3-ethylbenzothiazoline-6-sulphonic acid)
Ara	arabinose
BP	biological process
CAT	catalase
CC	cellular composition
DAGs	directed acyclic graphs

DEGs	differentially expressed genes
DPPH	1,1-diphenyl-2-picrylhydrazyl
EMP	exopolysaccharides produced in medium without genistein
EPS	exopolysaccharides
FDR	false discovery rate
Gal	galactose
GalA	galacturonic acid
G-EMP	exopolysaccharides produced in medium supplemented with genistein
Glc	glucose
GlcA	glucuronic acid
GO	gene ontology
GPI	glucose-6-phosphate isomerase
GSH	reduced glutathione
HK	hexokinase
KEGG	Kyoto Encyclopedia of Genes and Genomes
Man	mannose
MF	molecular function
MPI	mannose-6-phosphate isomerase
Mw	molecular weight
pmg	phosphoglucomutase
Rha	rhamnose
RNA-seq	RNA sequencing
ROS	reactive oxygen species
SEM	scanning electron microscopy
SmF	submerged fermentation
SOD	superoxide dismutase
Vc	ascorbic acid
Xyl	xylose

Appendix A. Supplementary data

Supplementary data to this article can be found online at https://doi.org/10.1016/j.crfs.2022.11.011.

References

Agbenorhevi, J.K., Kontogiorgos, V., Kirby, A.R., Morris, V.J., Tosh, S.M., 2011. Rheological and microstructural investigation of oat beta-glucan isolates varying in molecular weight. Int. J. Biol. Macromol. 49 (3), 369–377.

Bhawal, S., Kumari, A., Kapila, S., Kapila, R., 2021. Physicochemical characteristics of novel cell-bound exopolysaccharide from Probiotic *Limosilactobacillus* fermentum (MTCC 5898) and its relation to antioxidative activity. J. Agric. Food Chem. 69, 10338–10349.

Bol, M., Schrinner, K., Tesche, S., Krull, R., 2021. Challenges of influencing cellular morphology by morphology engineering techniques and mechanical induced stress on filamentous pellet systems-A critical review. Eng. Life Sci. 21 (3–4), 51–67.

Cao, Y.Y., Ji, Y.H., Liao, A.M., Huang, J.H., Thakur, K., Li, X.L., Wei, Z.J., 2020. Effects of sulfated, phosphorylated and carboxymethylated modifications on the antioxidant activities in-vitro of polysaccharides sequentially extracted from *Amana edulis*. Int. J. Biol. Macromol. 146, 887–896.

Chauton, M.S., Winge, P., Brembu, T., Vadstein, O., Bones, A.M., 2013. Gene regulation of carbon fixation, storage, and utilization in the diatom *Phaeodactylum tricornutum* acclimated to light/dark cycles. Plant Physiol. 161 (2), 1034–1048.

Chen, X., Yang, J., Shen, M., Chen, Y., Yu, Q., Xie, J., 2022a. Structure, function and advance application of microwave-treated polysaccharide: a review. Trends Food Sci. Technol. 123, 198–209.

Chen, S., Qin, L., Xie, L., Yu, Q., Chen, Y., Chen, T., Xie, J., 2022b. Physicochemical characterization, rheological and antioxidant properties of three alkali-extracted polysaccharides from mung bean skin. Food Hydrocolloids 132, 107867.

Coconi-Linares, N., Ortiz-Vazquez, E., Fernandez, F., Loske, A.M., Gomez-Lim, M.A., 2015. Recombinant expression of four oxidoreductases in *Phanerochaete chrysosporium* improves degradation of phenolic and non-phenolic substrates. J. Biotechnol. 209, 76–84.

Cui, F.J., Chen, X.X., Liu, W.M., Sun, W.J., Huo, S., Yang, Y., 2016. Control of *Grifola frondosa* morphology by agitation and aeration for improving mycelia and exo-polymer production. Appl. Biochem. Biotechnol. 179 (3), 459–473.

Ding, M., Liu, Y., Ye, Y.F., Zhang, J.C., Wang, J.H., 2021. Polysaccharides from the lignified okra: physicochemical properties and rheological properties. Carbohydr Diet Fibre 26, 100274.

Fang, Y., Huang, B., Zhang, Y., Liu, H., Zou, C., 2022. Polysaccharide derived from pomelo seed coat ameliorates APA-induced liver injury in hybrid grouper (*Epinephelus lanceolatus♂×Epinephelus fuscoguttatus♀*). eFood 2 (6), 319–325.

Feng, X., Li, Y., Brobbey Oppong, M., Qiu, F., 2018. Insights into the intestinal bacterial metabolism of flavonoids and the bioactivities of their microbe-derived ring cleavage metabolites. Drug Metab. Rev. 50 (3), 343–356.

Hamers, T., Kamstra, J.H., Sonneveld, E., Murk, A.J., Visser, T.J., Van Velzen, M.J., Bergman, A., 2008. Biotransformation of brominated flame retardants into potentially endocrine-disrupting metabolites, with special attention to 2,2',4,4'-tetrabromodiphenyl ether (BDE-47). Mol. Nutr. Food Res. 52 (2), 284–298.

Hasheminya, S.-M., Dehghannya, J., 2020. Novel ultrasound-assisted extraction of kefiran biomaterial, a prebiotic exopolysaccharide, and investigation of its physicochemical, antioxidant and antimicrobial properties. Mater. Chem. Phys. 243, 122645.

Hou, C., Chen, L., Yang, L., Ji, X., 2020. An insight into anti-inflammatory effects of natural polysaccharides. Int. J. Biol. Macromol. 153, 248–255.

Hsieh, C., Wang, H.-L., Chen, C.-C., Hsu, T.-H., Tseng, M.-H., 2008. Effect of plant oil and surfactant on the production of mycelial biomass and polysaccharides in submerged culture of *Grifola frondosa*. Biochem. Eng. J. 38 (2), 198–205.

Hu, Y.H., Ge, M.D., Sun, D.N., Chen, L., Cheung, P.C.K., You, C.P., Ng, H., 2022a. Stimulating mechanism of corn oil on biomass and polysaccharide production of *Pleurotus tuber-regium* mycelium. Int. J. Biol. Macromol. 201, 93–103.

Hu, X., Pan, Y., Bao, M., Zhang, X., Luo, C., Han, X., Li, F., 2022b. The structure, properties and rheological characterisation of exopolysaccharides produced by *Chryseobacterium cucumeris* AP-2 from deteriorated milk. Int. Dairy J. 126, 105253.

Huang, Z., Zhang, L., Wang, Y., Gao, H., Li, X., Huang, T., 2019. Effects of rutin and its derivatives on citrinin production by *Monascus aurantiacus* Li AS3.4384 in liquid fermentation using different types of media. Food Chem. 284, 205–212.

Ji, X., Hou, C., Yan, Y., Shi, M., Liu, Y., 2020. Comparison of structural characterization and antioxidant activity of polysaccharides from jujube (*Ziziphus jujuba* Mill.) fruit. Int. J. Biol. Macromol. 149, 1008–1018.

Jiang, N., Wang, L., Jiang, D., Wang, M., Liu, H., Yu, H., Yao, W., 2022. Transcriptomic analysis of inhibition by eugenol of ochratoxin A biosynthesis and growth of *Aspergillus carbonarius*. Food Control 135, 108788.

Liu, H., Xie, M., Nie, S., 2020a. Recent trends and applications of polysaccharides for microencapsulation of probiotics. Food Frontiers 1 (1), 45–59.

Liu, J., Wang, Y., Wu, J., Georgiev, M.I., Xu, B., Wong, K.H., Tian, L., 2022. Isolation, structural properties, and bioactivities of polysaccharides from mushrooms *Termitomyces*. J. Agric. Food Chem. 70 (1), 21–33.

Liu, M., Yang, L., Cai, M., Feng, C., Zhao, Z., Yang, D., Ding, P., 2021. Transcriptome analysis reveals important candidate gene families related to oligosaccharides biosynthesis in Morindaofficinalis. Plant Physiol. Biochem. 167, 1061–1071.

Liu, S., Xie, L., Shen, M., Xiao, Y., Yu, Q., Chen, Y., Xie, J., 2020b. Dual modifications on the gelatinization, textural, and morphology properties of pea starch by sodium carbonate and *Mesona chinensis* polysaccharide. Food Hydrocolloids 102, 105601.

Meng, Q., Chuai, S., Chen, L., Wang, L., Cai, G., Mao, J., Ding, Z., 2021. Effect of surfactants on the production of polysaccharides from *Schizophyllum* commune through submerged fermentation. Int. J. Biol. Macromol. 192, 210–218.

Miura, Y., Fulco, A.J., 1974. (ω-2) hydroxylation of fatty acids by a soluble system from Bacillus megaterium. J. Biol. Chem. 249 (6), 1880–1888.

Nwodo, U.U., Green, E., Okoh, A.I., 2012. Bacterial exopolysaccharides: functionality and prospects. Int. J. Mol. Sci. 13 (11), 14002–14015.

Peng, L., Qiao, S., Xu, Z., Guan, F., Ding, Z., Gu, Z., Shi, G., 2015. Effects of culture conditions on monosaccharide composition of *Ganoderma lucidum* exopolysaccharide and on activities of related enzymes. Carbohydr. Polym. 133, 104–109.

Peng, X., Yu, Q., Liu, Y., Ma, T., Li, M., 2020. Study on the function of the inositol polyphosphate kinases kcs1 and vip1 of *candida albicans* in energy metabolism. Front. Microbiol. 11, 566069.

Roux, C., Gresh, N., Perera, L.E., Piquemal, J.P., Salmon, L., 2007. Binding of 5-phospho-D-arabinonohydroxamate and 5-phospho-D-arabinonate inhibitors to zinc phosphomannose isomerase from Candida albicans studied by polarizable molecular mechanics and quantum mechanics. J. Comput. Chem. 28 (5), 938–957.

Scervino, J.M., Ponce, M.A., Erra-Bassells, R., Vierheilig, H., Ocampo, J.A., Godeas, A., 2005. Flavonoids exhibit fungal species and genus specific effects on the presymbiotic growth of *Gigaspora* and *Glomus*. Mycol. Res. 109 (Pt 7), 789–794.

Silva, L.A., Lopes Neto, J.H.P., Cardarelli, H.R., 2019. Exopolysaccharides produced by *Lactobacillus plantarum*: technological properties, biological activity, and potential application in the food industry. Ann. Microbiol. 69 (4), 321–328.

Sirin, S., Aslim, B., 2021. Protective effect of exopolysaccharides from lactic acid bacteria against amyloid beta1-42induced oxidative stress in SH-SY5Y cells: involvement of the AKT, MAPK, and NF-κB signaling pathway. Process Biochem. 106, 50–59.

Wang, J., Liang, J., Li, Y., Tian, L., Wei, Y., 2021. Characterization of efficient xylanases from industrial-scale pulp and paper wastewater treatment microbiota. Amb. Express 11 (1), 19.

Wang, Z., Sun, Q., Zhang, H., Wang, J., Fu, Q., Qiao, H., Wang, Q., 2021a. Insight into antibacterial mechanism of polysaccharides: a review. Lebensm. Wiss. Technol. 150, 111929.

Wang, L., Li, L., Gao, J., Huang, J., Yang, Y., Xu, Y., Yu, W., 2021b. Characterization, antioxidant and immunomodulatory effects of selenized polysaccharides from dandelion roots. Carbohydr. Polym. 260, 117796.

Wang, Z., Zhu, J., Li, W., Li, R., Wang, X., Qiao, H., Zhang, H., 2020. Antibacterial mechanism of the polysaccharide produced by *Chaetomium globosum* CGMCC 6882 against *Staphylococcus aureus*. Int. J. Biol. Macromol. 159, 231–235.

Xie, L., Huang, Z., Meng, H., Shi, X., Xie, J., 2022. Immunomodulation effect of polysaccharides from liquid fermentation of *Monascus purpureus* 40269 via membrane TLR-4 to activate the MAPK and NF-kappaB signaling pathways. Int. J. Biol. Macromol. 201, 480–491.

Xie, L., Huang, Z., Meng, H., Fan, Z., Shi, X., Xie, J., 2022a. Role of genistein on the yield, structure and immunomodulatory activity of *Monascus* exopolysaccharides. Food Funct. 13, 1393–1407.

Xie, L., Huang, Z., Qin, L., Yu, Q., Chen, Y., Zhu, H., Xie, J., 2022b. Effects of sulfation and carboxymethylation on *Cyclocarya paliurus* polysaccharides: physicochemical properties, antitumor activities and protection against cellular oxidative stress. Int. J. Biol. Macromol. 204, 103–115.

Xie, L., Shen, M., Wen, P., Hong, Y., Liu, X., Xie, J., 2020. Preparation, characterization, antioxidant activity and protective effect against cellular oxidative stress of phosphorylated polysaccharide from *Cyclocarya paliurus*. Food Chem. Toxicol. 145, 111754.

Xie, L., Shen, M., Wang, Z., Xie, J., 2021. Structure, function and food applications of carboxymethylated polysaccharides: a comprehensive review. Trends Food Sci. Technol. 118, 539–557.

Xu, X., Wu, P., Wang, T., Yan, L., Lin, M., Chen, C., 2019. Synergistic effects of surfactant-assisted biodegradation of wheat straw and production of polysaccharides by Inonotus obliquus under submerged fermentation. Bioresour. Technol. 278, 43–50.

Yang, H., Min, W., Bi, P., Zhou, H., Huang, F., 2013. Stimulatory effects of Coix lacryma-jobi oil on the mycelial growth and metabolites biosynthesis by the submerged culture of Ganoderma lucidum. Biochem. Eng. J. 76, 77–82.

Ye, Y., Ling, N., Jiao, R., Wu, Q., Han, Y., Gao, J., 2015. Effects of Ca^{2+} and Mg^{2+} on the biofilm formation of *Cronobacter Sakazakii* strains from powdered infant formula. J. Food Saf. 35 (3), 416–421.

Yuan, D., Li, C., Huang, Q., Fu, X., 2020. Ultrasonic degradation effects on the physicochemical, rheological and antioxidant properties of polysaccharide from *Sargassum pallidum*. Carbohydr. Polym. 239, 116230.

Zhang, B.B., Cheung, P.C., 2011. A mechanistic study of the enhancing effect of Tween 80 on the mycelial growth and exopolysaccharide production by *Pleurotus* tuber-regium. Bioresour. Technol. 102 (17), 8323–8326.

Zhu, F., Li, J., Ma, Z., Li, J., Du, B., 2021. Structural identification and *in vitro* antioxidant activities of anthocyanins in black chokeberry (*Aronia melanocarpa* lliot). eFood 2 (4), 201–208.